12th International Symposium on Turbulence and Shear Flow Phenomena (TSFP12)
Osaka, Japan (Online), July 19-22, 2022

INVESTIGATIONS OF VORTEX SHEDDING AND FLAME BASE FLUCTUATIONS IN A DUAL SWIRL BURNER USING SPIV, OH PLIF AND CHEMILUMINESCENCE

Masayasu Shimura
Department of Mechanical Engineering
Tokyo Institute of Technology
2-12-1 Ookayama, Meguro-ku,
Tokyo 152-8550 Japan
shimura.m.aa@m.titech.ac.jp

Hiroki Hattori
Department of Mechanical Engineering
Tokyo Institute of Technology
2-12-1 Ookayama, Meguro-ku,
Tokyo 152-8550 Japan
shimura.m.aa@m.titech.ac.jp

Mamoru Tanahashi
Department of Mechanical Engineering
Tokyo Institute of Technology
2-12-1 Ookayama, Meguro-ku, Tokyo 152-8550 Japan
shimura.m.aa@m.titech.ac.jp

ABSTRACT

Simultaneous high-speed measurements of stereoscopic particle image velocimetry (SPIV), OH planer laser induced fluorescence (OH-PLIF), and OH chemiluminescence were conducted in order to investigate relationship between fluctuation of flame base and flow structure in a dual-swirl burner, in which peak frequency of fluctuations of flame base changes according to equivalence ratio and the ratio of outer and inner air swirl flow rates. Flame base is defined by height of upstream edge of OH chemiluminescence. Spectral analysis on temporal data of flame base fluctuation and velocity revealed one of major factors of flame base fluctuation. The flame base is located in the shear layer between the inflow gas and the inner recirculation zone (IRZ). The velocity spectra show that the mainstream and radial velocity components have the same peak frequency as fluctuations of the lift-off height in the same locations. It is also found that the peak frequency is proportional to the magnitude of the mean velocity gradient at the mean flame base position. Finally it is found that the Strouhal number based on characteristics of shear layer between inner swirl flow and inner recirculation zone was found to be constant regardless of the total flow rate and the flow rate ratio.

INTRODUCTION

For the gas turbine combustors utilized widely as propulsion engines and power generation systems, non-premixed and partially premixed combustion are widely used because of no risk of flash back and easiness of control. Some of gas turbine combustors have coaxial dual swirl flows, which is called dual swirl burner hereafter, to stabilize flame and to enhance mixing of fuel and air. For the DLR dual swirl burner, Weigand et al. (2006) conducted laser Doppler velocimetry (LDV) and OH/CH-planar laser induced fluorescence (PLIF) and revealed that intense velocity fluctuations occur in the shear layer between the inner recirculation zone (IRZ) and influent gas and reaction zone are strongly corrugated. Meier et al. (2006) conducted laser Raman scattering and reported that the unreacted or partial-reacted gas exists in the same region because of local flame extinction and ignition delay. Stöhr et al. (2012) have conducted particle image velocimetry (PIV) and OH PLIF at 5 kHz and found that precessing vortex core (PVC) induces an unsteady lower stagnation point. Oscillation characteristics of the dual swirl burner was investigated using large eddy simulation (LES) Chen et al. (2019) and it is revealed that variations of air mass split rate between dual swirl flows are significant on fuel-air mixing characteristics in thermoacoustic oscillation cycles. Recently, Litvinov et al. (2021) have investigated mixing and reaction characteristics in the dual swirl burner with separately supplied air flows by using time-resolved stereo-PIV, OH-PLIF and acetone-PLIF and revealed that PVC and double helical vortex are generated in inner and outer shear layer and cause flame roll-up, mixing of burnt and unburnt gases and subsequent ignition both in the inner and outer shear layers. PVC and fluctuations of recirculation zones in swirl burners have been studied. Oscillation mechanism due to PVC were reviewed by Syred (2006).

In many previous studies, the ratio of two swirl flow rates has not been set arbitrarily, and hence effect on the characteristics of turbulence and mixing of air and fuel in the shear layer have not been well discussed. Therefore, in our research project, a dual swirl burner in which the ratio of two swirl flow rates is adjustable is constructed. The objectives of this study are to clarify the effects of the air flow ratio on the characteristics of flame base fluctuation and a major factor causing flame base fluctuation by using stereoscopic PIV, OH-PLIF, and OH chemiluminescence measurement.

EXPERIMENTAL SETUP

Figure 1 shows a schematic of dual swirl burner used in this study. The nozzles are co-axial triple cylinders for air, methane, and air in order from the inside. Both of the two air nozzles are equipped with swirlers whose blade angle is 45

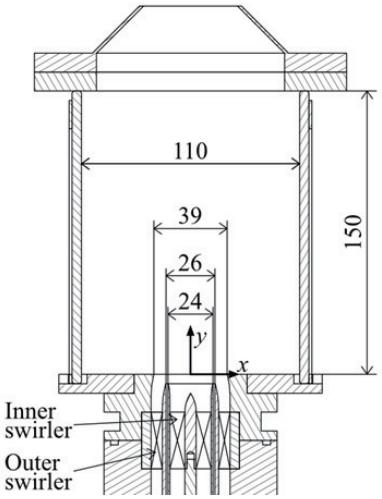

Figure 1. Schematic of a dual swirl burner.

degrees to the center axis, and inner swirl flow is clockwise and the outer swirl flow is counter clockwise viewed from the negative region of the y axis. The diameters of the nozzles are 24 mm, 26 mm and 39 mm, respectively and the outlet of the inner air and fuel nozzle are located 5 mm upstream from the bottom of the chamber. A combustion chamber has a cross-section of 110 mm $\times$ 110 mm and a height of 150 mm, the sides are covered with quartz glass, which enables optical measurements.

Figure 2 shows a schematic of simultaneous SPIV and OH chemiluminescence measurements system. In SPIV, 532 nm laser beam emitted from two Nd:YAG laser (Lee Laser LDP-100MQG) is double-pulsed using a 1/2 wave plate and polarizing beam splitter turned into a sheet and the guided to a cross-section including center axis of the burner. SiO_2 tracer particles (Suzukiyushi Industrial Corporation, E-6C) with an average diameter of 2 μm ware seeded in two air swirl flow respectively, and scattered light from the particles was captured by two high-speed CMOS cameras (Photron, SA-Z) through and macro lenses (Nikon, AF Micro-Nikkor 200 mm f/4D IF-ED) and optical filters (Edmund Optics, LONGPASS FILTER BP center: 525 nm, band width: 50 nm). Three components velocity was obtained at 10 kHz.

In OH-PLIF, Nd:YAG laser (Edgewave, IS120-2-L, 532 nm, 5 mJ/pulse) and dye laser (LIOPTEC, LiopStar-HQ, Rhodamine 6G) were used. In this study, $Q_1(7)$ absorption line in the (1,0) vibrational band of $A^2\Sigma - X^2\Pi$ electronic transition at a wavelength of around 283 nm was used to excite OH radical and fluorescence in the (1,1) and (0,0) vibrational bands of A-X transition in range of 306-320 nm was detected. The pulse energy was 45 μJ/pulse. Laser beam was aligned with that of SPIV laser using dichroic mirror and guided to the measurement area in the form of a sheet. The OH radical fluorescence was detected by a UV macro lens (Sodern, 100 mm F/2.8 type CERCO 2178) equipped with a bandpass filter with a center wavelength of 320 nm and a half maximum full-width of 44 nm (Semrock, FF01-320/40-50-D), amplified by an image intensifier (I.I.) (Hamamatsu Photonics, C10880-03F), and recorded by a CMOS camera (nac, Memrecam ACS-3). The gate width and gain of I.I. was set at 40 ns and 770, respectively.

In OH chemiluminescence measurement, the light emitted from the flame was captured by a UV-compatible lens equipped with a bandpass filter, amplified by an image intensifier, and recorded by CMOS camera (Photron, SA-X2). A

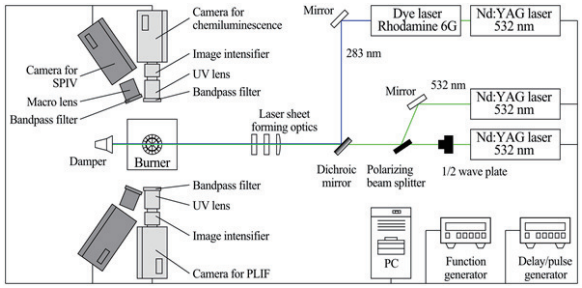

Figure 2. Experimental setup of simultaneous stereoscopic PIV, OH-PLIF, and OH chemiluminescence.

Table 1. Experimental conditions of total mass flow rate, Q_t [L/min], ratio of mass flow rates of inner and outer air flow, Q_o/Q_i, and bulk velocities of inner and outer air flow (V_i [m/s] and V_o [m/s]) and fuel flow (V_f [m/s]).

Q_t	Q_o/Q_i	V_i	V_o	V_f
300	1.6	5.09	3.00	4.35
300	2.0	4.41	3.25	4.35
300	2.4	3.89	3.44	4.35
400	1.6	6.79	4.00	5.79
400	2.0	5.88	4.34	5.79
400	2.4	5.19	4.59	5.79
500	1.6	8.49	5.00	7.26
500	2.0	7.36	5.42	7.26
500	2.4	6.49	5.74	7.26

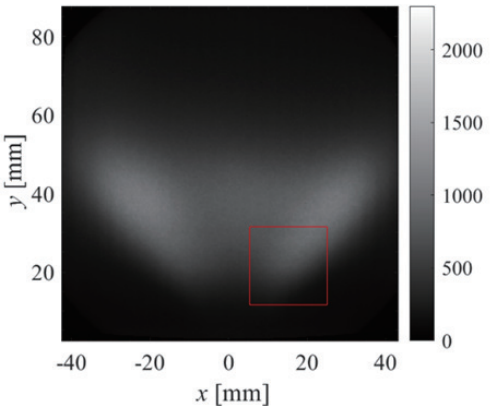

Figure 3. Mean distribution of OH chemiluminescence at total flow rate of 300 L/min and flow rate ratio of 2.0 and measurement area of SPIV and OH-PLIF (red line)

delay pulse generator (Photron, SA-X2) was used to synchronize the camera and I.I., and waveform generator (Keysight Technology, 33512B) was use to trigger the start of the measurements.

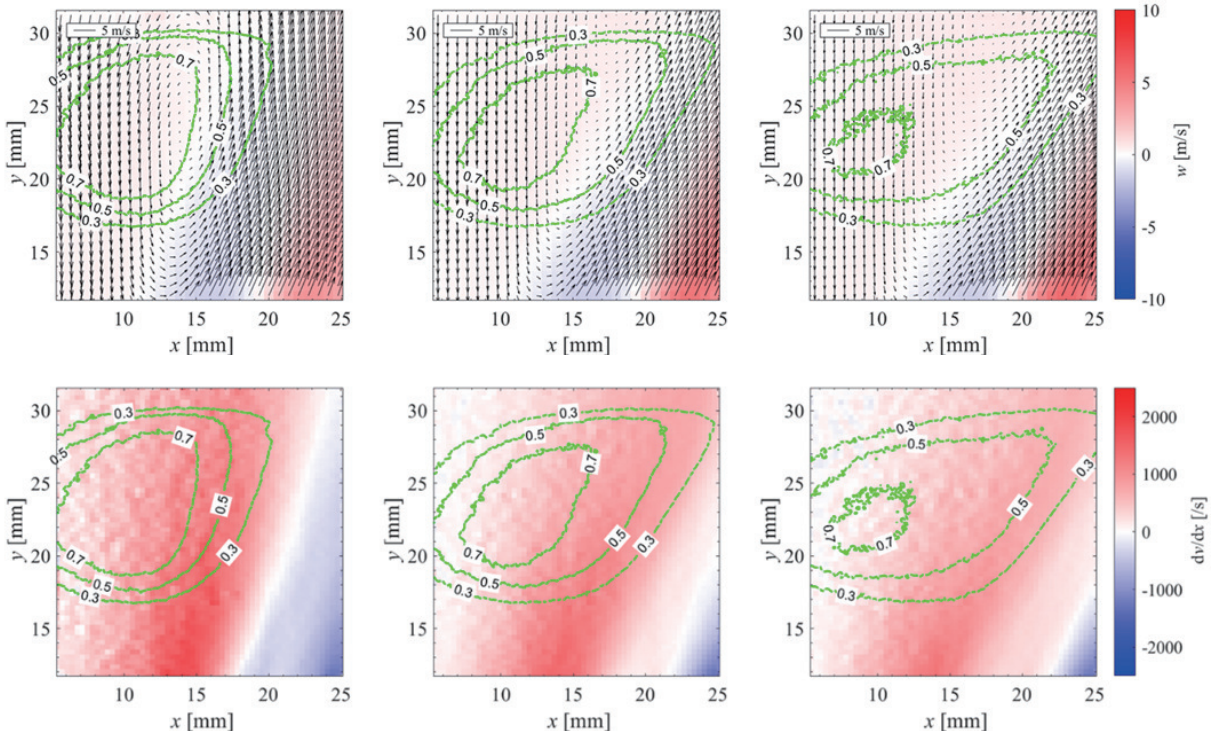

Figure 4. Mean distributions of velocity (a) and dv/dx (b) with contour lines of OH radical existence probability of 30%, 50% and 70% (green lines) at flow rate ratio of 1.6, 2.0 and 2.4 from the left for 300 L/min.

Experimental and Measurement Conditions

The equivalence ratio was fixed at 0.70. Total flow rate was set at 300 L/min, 400 L/min, and 500 L/min. Experimental conditions of total mass flow rate, Q_t [L/min], ratio of mass flow rates of inner and outer air flow, Q_o/Q_i, and bulk velocities of inner and outer air flow (V_i [m/s] and V_o [m/s]) and fuel flow (V_f [m/s]) are listed in Table 1. To investigate the characteristics of the flame base in relation to the flow ratio, the ratio of the outer air flow to the inner air flow rate were set at 1.6, 2.0 and 2.4. Table 1 shows the bulk flow velocity for each condition.

Figure 3 shows the mean distribution of OH chemiluminescence at a flow rate ratio of 2.0 and the measurement area of SPIV. The measurement area of SPIV and OH-PLIF was 19.7 mm $\times$ 19.9 mm (5.4 mm $< x <$ 25.1 mm, 11.7 mm $< y <$ 31.6 mm) near the flame base. However, a region with laser intensity sufficient for OH excitation is limited in about 18 mm $< y <$ 28 mm.

The camera resolutions are 79 μm $\times$ 79 μm for OH-PLIF, 111 μm $\times$ 111 μm for OH chemiluminescence and 21 μm $\times$ 21 μm for PIV. Time separation of successive images of PIV was 6.6 μs. The spatial resolution of PIV, which was defined as the size of interrogation region, is 672 μm $\times$ 672 μm, while vector spacing is 336 μm $\times$ 336 μm. Laser sheet thickness for OH-PLIF and PIV is 305 μm and 393 μm, respectively.

In order to evaluate the dynamic characteristics of the flame base fluctuation, it is necessary to define the lift-off height. In this study, the lift-off height was defined as the lowest point of the OH region captured by the OH chemiluminescence, based on the method of Degeneve et al. (2021). Otsu method was used for the discrimination of OH existence (Otsu, 1984). The lift-off height was calculated in each of the $x > 0$ and $x < 0$ regions. Mean and rms values of lift-off height (h_m [mm] and h'_{rms} [mm]) and peak frequency of flame base fluctuations (f_p [Hz]) (lift-off height fluctuations) are listed in

Table 2. Characteristics of lift-off height fluctuations.

Q_t	Q_o/Q_i	h_m	h'_{rms}	f_p
300	1.6	15.4	3.14	224.6
300	2.0	14.6	2.80	195.3
300	2.4	14.3	2.80	166.0
400	1.6	15.5	3.12	312.5
400	2.0	14.7	2.73	273.4
400	2.4	14.9	2.70	239.3
500	1.6	16.6	2.51	439.5
500	2.0	14.6	2.48	341.8
500	2.4	13.9	2.36	278.3

Table 2.

RESULTS AND DISCUTTIONS

Figure 4 shows distributions of mean velocity and contours of 30%, 50%, and 70% existence probability of OH fluorescence for 300 L/min case. It can be seen that at the average flame base location, there is a large velocity gradient is generated by inflow gas and IRZ. The out-of-plane velocity component shows a large gradient in a shear layer between the inner and outer swirl flows. The shear layer between the inner swirl flow and the IRZ also show the large out-of-plane velocity gradient in the radial direction, where the edge region of OH radicals is located. As shown in Fig. 10, the reaction zone

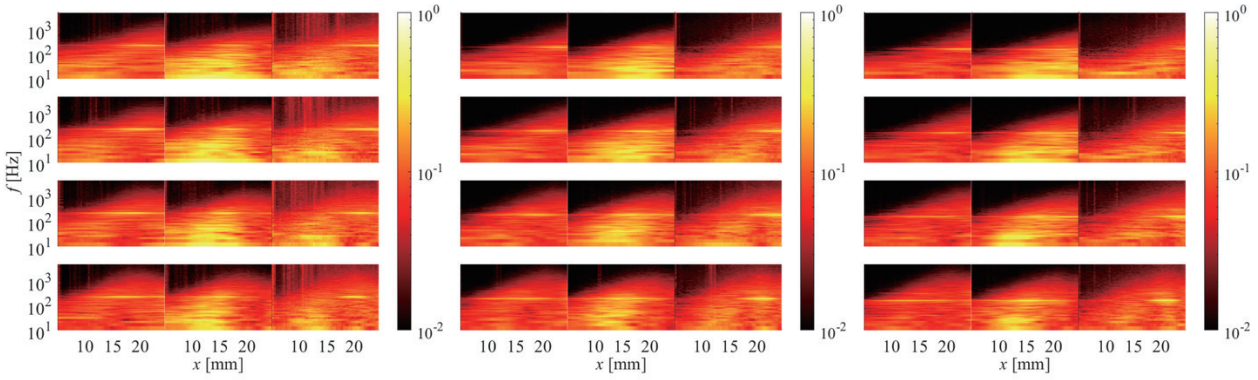

Figure 5. The velocity spectra at heights of $y = 30$ mm, 25 mm, 20 mm, and 15 mm at total flow rate of 300 L/min and the flow rate ratio of 1.6, 2.0 and 2.4 from the left. Left, middle, and right columns are radial, mainstream and out-of-plane components of velocity, respectively.

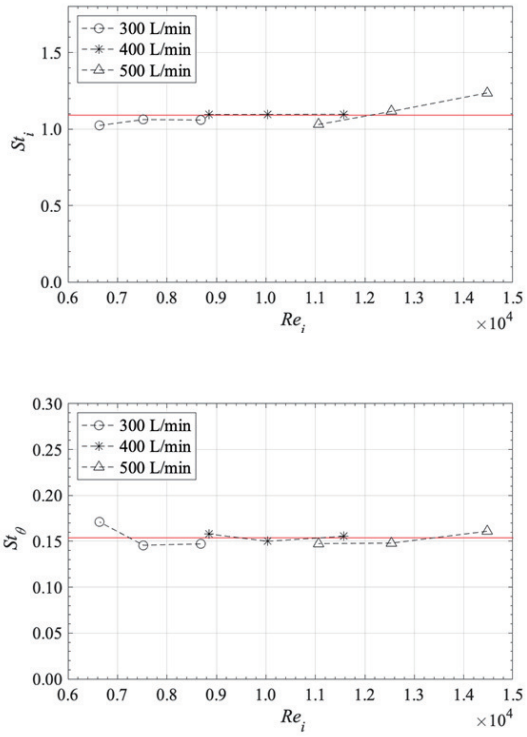

Figure 6. Strouhal number defined by bulk velocity and inner nozzle diameter (top) and one defined by velocity gradient versus Reynolds number (bottom).

is engulfed by the vortex generated in the shear layer. At $y =$ 20 mm $\sim$ 25 mm, width between 30% and 50% lines of OH radical existence is nearly same for the conditions tested. On the other hand, width between 50% and 70% lines depends on the flow rate ratio conditions, and that is large for the larger flow rate ratio. However, this does not necessarily represent less stability of inner recirculation zone, because higher flow rate ratio has larger IRZ and OH radical is possible to be more consumed in longer resident time. The consumption of OH radical in the inner recirculation zone also causes a small region of OH existence higher than 70%.

Figure 4 also shows distributions of mean dv/dx and contours of 30%, 50%, and 70% existence probability of OH fluorescence. Velocity gradients were calculated using a fourth-order central difference scheme for velocity data smoothed by 3000 Hz cutoff filter. The absolute values of velocity gradients of dv/dx are strongly correlated with the peak frequency of the lift-off height. The shear layer generated between IRZ and the inner air flow tends to have large velocity difference for lower flow rate ratio and large velocity gradient at the location of average flame base, which results in higher frequency of vortex shedding.

Figure 5 shows velocity spectra at heights of y = 15 mm, 20 mm, 25 mm, and 30 mm at the flow rate ratio of 1.6, 2.0 and for $Q_t = 300$ L/min. All the velocity components have a peak frequency same as that of lift-off height specific to the flow rate ratio. The spectra of the mainstream and radial velocity components have peaks near the average flame base position, while the out-of-plane velocity component has peaks in the shear layer between the inner and outer air flows. It can be concluded that the fluctuation of lift-off height is caused by the intermittent motion of shear turbulence between the inflow and the IRZ.

Figure 6 shows the Strouhal numbers with respect to the Reynolds number Re_i defined by the bulk velocity V_i, outer diameter of inner swirl flow inlet D_i and kinematic viscosity of air at 298 K. The Strouhal numbers are defined as:

$$St_i = f_p D_i / V_i \tag{1}$$

$$St_\theta = f_p / (dv/dx)_{LMAX} \tag{2}$$

In Fig. 6, St_i tenda to increase with increase of Re_i in high Reynolds number region. This is caused by the change of swirl numbe, and is consistent with the literatures by Syred (2006) and Stohr et al. (2012). Note that the increase trend of St_i is very weak. On the other hand, St_θ has nearly constant value in $Re_i > 7000$. The vortex shedding is caused by instability of inner shear layer, and hence the local maximum value of velocity gradient at the mean lift-off height works well for alignment of the frequency of lift-off height.

concludsions

Simultaneous high-speed measurements of stereoscopic particle image velocimetry (SPIV), OH planer laser induced fluorescence (OH-PLIF), and OH chemiluminescence were conducted in order to investigate relationship between fluctuation of flame base and flow structure in a dual-swirl burner,

in which peak frequency of fluctuations of flame base changes according to equivalence ratio and the ratio of outer and inner air swirl flow rates.

The frequency of vortex shedding was discussed based on velocity gradient at averaged location of lift-off height of the flames tested. The shear layer generated between inner recirculation zone (IRZ) and the inner air flow tends to have large velocity difference for lower flow rate ratio and large velocity gradient at the location of average flame base, which results in higher frequency of vortex shedding because of the instability of shear layer. It has been clarified that the Strouhal number based on the bulk velocity at the inner swirl and inner swirler diameter has a trend to increase with increase of inner swirl air flow rate, while the Strouhal number based on the velocity gradient tends to be a constant. Hence it can be concluded that the characteristic frequency of flame lift-off height can be predicted based on the velocity gradient at the averaged flame base.

Acknowledgements

This work was supported by Fostering Joint International Research (A) Grant Number 18KK0400.

REFERENCES

Chen, Z.X., Langella, I., Swaminathan, N., Stöhr, M., Meier, W., Kolla, H., 2019, "Large Eddy Simulation of a dual swirl gas turbine combustor: Flame/flow structures and stabilisation under thermoacoustically stable and unstable conditions", Combustion and Flame, Vol. 203, pp. 279-300.

Degeneve, A., Vicquelim, R., Mirat, C., Caudal, J., Schuller, T., 2021, "Impact of co- and counter-swirl on flow recirculation and liftoff of non-premixed oxy-flames above coaxial injectors", Proceedings of the Combustion Institute, Vol. 38(4), pp. 5501-5508.

Litvinov, I., Yoon, J., Noren, C., Stöhr, M., Boxx, I., Geigle, K.P., 2021, "Time-resolved study of mixing and reaction in an aero-engine model combustor at increased pressure", Combustion and Flame, Vol. 231, p. 111474.

Meier, W., Duan, X. R., and Weigand, P., 2006, "Investigations of swirl flames in a gas turbine model combustor: II. Turbulence-chemistry interactions", Combustion and Flame, Vol. 144(1–2), pp. 225–236.

Otsu, N., 1979, "A Threshold Selection Method from Gray-Level Histograms", IEEE Transaction on Systems, Man and Cybernetics, Vol. 20(1), pp. 62–66.

Stöhr, M., Boxx, I., Carter, C. D., Meier, W., 2012, "Experimental study of vortex-flame interaction in a gas turbine model combustor", Combustion and Flame, Vol. 159, pp. 2636–2649.

Syred, N., 2006, "A review of oscillation mechanisms and the role of the precessing vortex core (PVC) in swirl combustion systems", Progress in Energy and Combustion Science, Vol. 32, pp. 93–161.

Weigand, P., Meier, W., Duan, X. R., Stricker, W., and Aigner, M., 2006, "Investigations of swirl flames in a gas turbine model combustor: I. Flow field, structures, temperature, and species distributions.", Combustion and Flame, Vol. 144(1–2), pp. 205–224.